


A genome-wide screen identifies IRF2 as a key regulator of caspase-4 in human cells

Sacha Benaoudia¹, Amandine Martin¹, Marta Puig Gamez^{2,3,4,5}, Gabrielle Gay¹, Brice Lagrange¹, Maxence Cornut¹, Kyrilo Krasnykov¹, Jean-Baptiste Claude⁶, Cyril F Bourgeois⁶, Sandrine Hughes⁷, Benjamin Gillet⁷, Omran Allatif^{1,8}, Antoine Corbin^{1,8}, Romeo Ricci^{2,3,4,5} & Thomas Henry^{1,*} 

Abstract

Caspase-4, the cytosolic LPS sensor, and gasdermin D, its downstream effector, constitute the non-canonical inflammasome, which drives inflammatory responses during Gram-negative bacterial infections. It remains unclear whether other proteins regulate cytosolic LPS sensing, particularly in human cells. Here, we conduct a genome-wide CRISPR/Cas9 screen in a human monocyte cell line to identify genes controlling cytosolic LPS-mediated pyroptosis. We find that the transcription factor, IRF2, is required for pyroptosis following cytosolic LPS delivery and functions by directly regulating caspase-4 levels in human monocytes and iPSC-derived monocytes. *CASP4*, *GSDMD*, and *IRF2* are the only genes identified with high significance in this screen highlighting the simplicity of the non-canonical inflammasome. Upon IFN- γ priming, *IRF1* induction compensates *IRF2* deficiency, leading to robust caspase-4 expression. Deficiency in *IRF2* results in dampened inflammasome responses upon infection with Gram-negative bacteria. This study emphasizes the central role of IRF family members as specific regulators of the non-canonical inflammasome.

Keywords caspase-11; inflammasome; interferon regulatory factor; lipopolysaccharide; LPS

Subject Categories Chromatin, Transcription & Genomics; Immunology; Microbiology, Virology & Host Pathogen Interaction

DOI 10.15252/embr.201948235 | Received 5 April 2019 | Revised 1 July 2019 | Accepted 10 July 2019 | Published online 29 July 2019

EMBO Reports (2019) 20: e48235

See also: **SJ Thygesen & KJ Stacey** (September 2019)

Introduction

Sepsis is a leading cause of mortality worldwide, accounting for over 5 million deaths annually [1]. Sepsis is a deregulated host response to severe infection and is characterized by life-threatening organ dysfunction [2]. While the deregulated host immune responses include both pro- and anti-inflammatory responses, the early deaths observed during sepsis are thought to be due to a systemic inflammatory response syndrome (SIRS) [3]. A prominent initiator of SIRS is lipopolysaccharide (LPS) [4], a component of the envelope of Gram-negative bacteria. This potent endotoxin engages several inflammatory receptors and is sufficient to trigger SIRS in both mice and humans [5,6].

Immune responses to LPS are induced following either extracellular recognition by TLR4 [7] or cytosolic recognition by caspase-4/5/11 [8–10]. While the TLR4 pathway was long thought to be the main pathway responsible for LPS-induced lethality [7], the discovery that caspase-11 is activated in mice in response to cytosolic LPS has shed a new light on LPS-induced pathologies [9,10]. Caspase-11 and its human homologues caspase-4 and 5 bind LPS and act both as receptor [8] and as effector of the so-called non-canonical inflammasomes [11]. Upon LPS binding, these inflammatory caspases oligomerize and become activated, leading to the cleavage of their substrate, gasdermin D [12,13]. Cleaved gasdermin D acts as a pore forming protein triggering an inflammatory form of cell death termed pyroptosis [14]. In addition, potassium efflux through gasdermin D pores activates NLRP3, leading to caspase-1 activation and subsequent release of IL-1 β and IL-18 [11,15–17]. In contrast to the TLR4 pathway, which has been well characterized and involves multiple proteins upstream and downstream of TLR4 [18], the description of the core complex involved in LPS cytosolic sensing is currently limited to two proteins: caspase-4 (and its homologues)

1 CIRI, Centre International de Recherche en Infectiologie, Inserm, U1111, Université Claude Bernard Lyon 1, CNRS, UMR5308, ENS de Lyon, Univ Lyon, Lyon, France

2 Institut de Génétique et de Biologie Moléculaire et Cellulaire (IGBMC), Centre National de la Recherche Scientifique, UMR 7104, Institut National de la Santé et de la Recherche Médicale U964, Université de Strasbourg, Illkirch, France

3 Laboratoire de Biochimie et de Biologie Moléculaire, Nouvel Hôpital Civil, Strasbourg, France

4 Université de Strasbourg, Strasbourg, France

5 INGESTEM National iPSC Infrastructure, Villejuif, France

6 LBMC, Laboratoire de Biologie et Modélisation de la cellule, Université Claude Bernard Lyon 1, INSERM U1210, CNRS, UMR5239, École Normale Supérieure de Lyon, Univ Lyon, Lyon, France

7 Sequencing Platform, Institut de Génétique Fonctionnelle de Lyon (IGFL), Université Claude Bernard Lyon 1, CNRS, UMR5242, École Normale Supérieure de Lyon, Univ Lyon, Lyon, France

8 BIBS, Bioinformatic and Biostatic Services, CIRI, Lyon, France

*Corresponding author. Tel: +33 4 3728 2372; E-mail: thomas.henry@inserm.fr

and gasdermin D [12]. Due to the relatively recent identification of this immune complex, it remains unclear whether additional factors regulate cytosolic LPS sensing by the non-canonical inflammasome [19]. Further, most studies characterizing the non-canonical inflammasome have employed mouse models, which do not fully recapitulate inflammasome activation in humans. In mice, cytoplasmic LPS sensing occurs by caspase-11, which differs from its human homologue, caspase-4, in several ways [20–25]. First, caspase-11 is highly inducible following engagement of the TLRs/TRIF pathways and/or IFN signaling [9,10,26,27]. In contrast, in human monocytes and macrophages, caspase-4 is constitutively expressed [28,29]. In addition, we recently demonstrated that caspase-4 detects under-acylated LPS [30] while murine macrophages did not respond to cytoplasmic delivery of under-acylated LPS [31]. The tetra-acylated LPS from *Francisella tularensis*, the agent of tularemia, is thus detected in human macrophages but does not trigger any inflammasome response in murine macrophages [30].

Here, we hypothesized that factors controlling cytosolic LPS-mediated pyroptosis remained to be identified in human monocytes. Using electroporation of *Francisella novicida* LPS and a CRISPR/cas9 genome-wide screen in U937 cells, we identified interferon regulatory factor 2 (*IRF2*) as one of the three human genes (together with *CASP4* and *GSDMD*) required for LPS-mediated pyroptosis in human cells. We further showed that under steady-state conditions, *IRF2* drives sensing of cytosolic LPS by directly controlling caspase-4 transcript levels; however, in the presence of IFN- γ , *IRF2* cooperates with *IRF1* to control the inflammasome responses to cytosolic LPS and Gram-negative bacteria. Our results thus provide insights into the regulation of caspase-4 in human cells at both steady state and during inflammation.

Results

A genome-wide screen identifies *IRF2*, gasdermin D, and caspase-4 as the three main players in LPS sensing

Prior to this report, two genome-wide CRISPR/cas9 screens have been performed to identify proteins involved in the cytosolic sensing of LPS. Both have been conducted in murine macrophage cell lines using *Escherichia coli* LPS [12,32]. To identify human-specific factors that may contribute to cytosolic detection of tetra-acylated LPS, we performed a genome-wide screen in U937 cells transfected with *F. novicida* LPS. A library of 76,441 sgRNA, in which each gene was targeted by four independent sgRNA [33], was introduced by transduction in U937 cells expressing spCas9 [30]. The obtained cell library was subsequently electroporated with 10 μ g of *F. novicida* LPS (a condition leading to approximately 40% cell death at 3 h post-transfection [30]). The surviving cells were then amplified over 4 days before going through another round of LPS electroporation. This cycle was repeated three times for a total of four electroporations (Fig 1A). SgRNA enrichment factors in the LPS-electroporated cells compared to the mock-electroporated cells were determined by next-generation sequencing to identify genes which knock-out impaired cell death/promoted cell survival following LPS electroporation. Strikingly, when focusing on the 10 most enriched sgRNAs, three genes—*IRF2*, *CASP4*, and *GSDMD*—were represented by several independent sgRNA (Fig 1B). Statistical analysis taking

into account the score of the four independent sgRNAs strengthened the prominent enrichment of these three genes (Fig 1C). Fifteen other genes were scored as significant although the corresponding adjusted *P*-values were at least 10^8 -fold greater than the adjusted *P*-values of *IRF2*, *CASP4*, and *GSDMD* (Table EV1). Overall, this genome-wide screen suggests that *IRF2* is a major player of *F. novicida* LPS cytosolic sensing in human cells.

To assess the role of all eighteen genes found to be significantly associated with cytosolic LPS sensing, we created stable cell lines using CRISPR/Cas9 and 2 sgRNA targeting each gene in U937 cells. Two of the identified genes (*PACS1* and *ZNF699*) did not pass the RNA-seq filtering step, indicating they are either not expressed, or poorly expressed in U937 cells (see Materials and Methods) (Fig EV1); therefore, they were not targeted. Following CRISPR/Cas9-mediated editing, three other candidate genes were excluded from further analyses due to either reduced growth rate of the mutated cell line (*TRIM28*), inefficient mutation (*DET1*), or a strong bias in insertions/deletions not causing a frameshift (*TFAP4*) (Appendix Table S1). Out of the 13 cell lines with validated open-reading frame disruptions (Appendix Table S1), the cell lines mutated for *IRF2* (Fig EV2A), *CASP4* [30], and *GSDMD* [30] demonstrated a drastic reduction in LDH release following LPS electroporation (Fig 1D). To further corroborate these results, we generated three independent *IRF2* knock-out (KO) cell lines and again observed a strong reduction in cell death upon LPS electroporation (Fig EV2A and B). Of note, since we observed that *IRF2* was required for LDH release in response to both *E. coli* and *F. novicida* LPS (Fig EV2C), we used *E. coli* LPS for subsequent experiments.

IRF2 is specifically required for caspase-4-mediated cell death

To confirm the role of *IRF2* in mediating pyroptosis following LPS electroporation, we first reconstituted physiological *IRF2* expression in *IRF2*^{KO} cells (Fig 2A). Importantly, ectopic expression of *IRF2* fully restored pyroptosis after LPS electroporation in *IRF2*^{KO} cells (Fig 2B and C), demonstrating that *IRF2* controls caspase-4-mediated pyroptosis.

We next sought to determine whether other IRFs could be involved in caspase-4-mediated pyroptosis. While several IRFs are involved in the regulation of various inflammasomes in mice [34,35], we did not observe a significant enrichment for any IRFs besides *IRF2* in our CRISPR/Cas9 screen (Fig 2D). Nine IRFs are present in humans. To exclude a possible role for other IRFs in caspase-4-mediated pyroptosis, we generated individual *IRF* mutated cell lines. Importantly, only *IRF2* mutations resulted in a significant reduction in LDH release upon LPS transfection (Fig 2E). This result suggests that *IRF2* is specifically required among IRF family members to regulate caspase-4-dependent pyroptosis.

To assess whether *IRF2* could be involved in other cell death pathways, we triggered necrosis using nigericin [36,37] and apoptosis using gliotoxin [38] or a staurosporine analogue, UCN-01 [39]. Of note, in the absence of phorbol 12-myristate 13-acetate (PMA)-mediated differentiation and LPS priming, we found nigericin-mediated necrosis in U937 cells to be independent of caspase-1 and gasdermin D (Appendix Fig S1). We monitored U937 cell death kinetics in real time using propidium iodide incorporation (Fig 2F). This technique confirmed the strong pyroptosis defect of *IRF2*^{KO} cells in response to LPS transfection (Fig 2B). However, we could

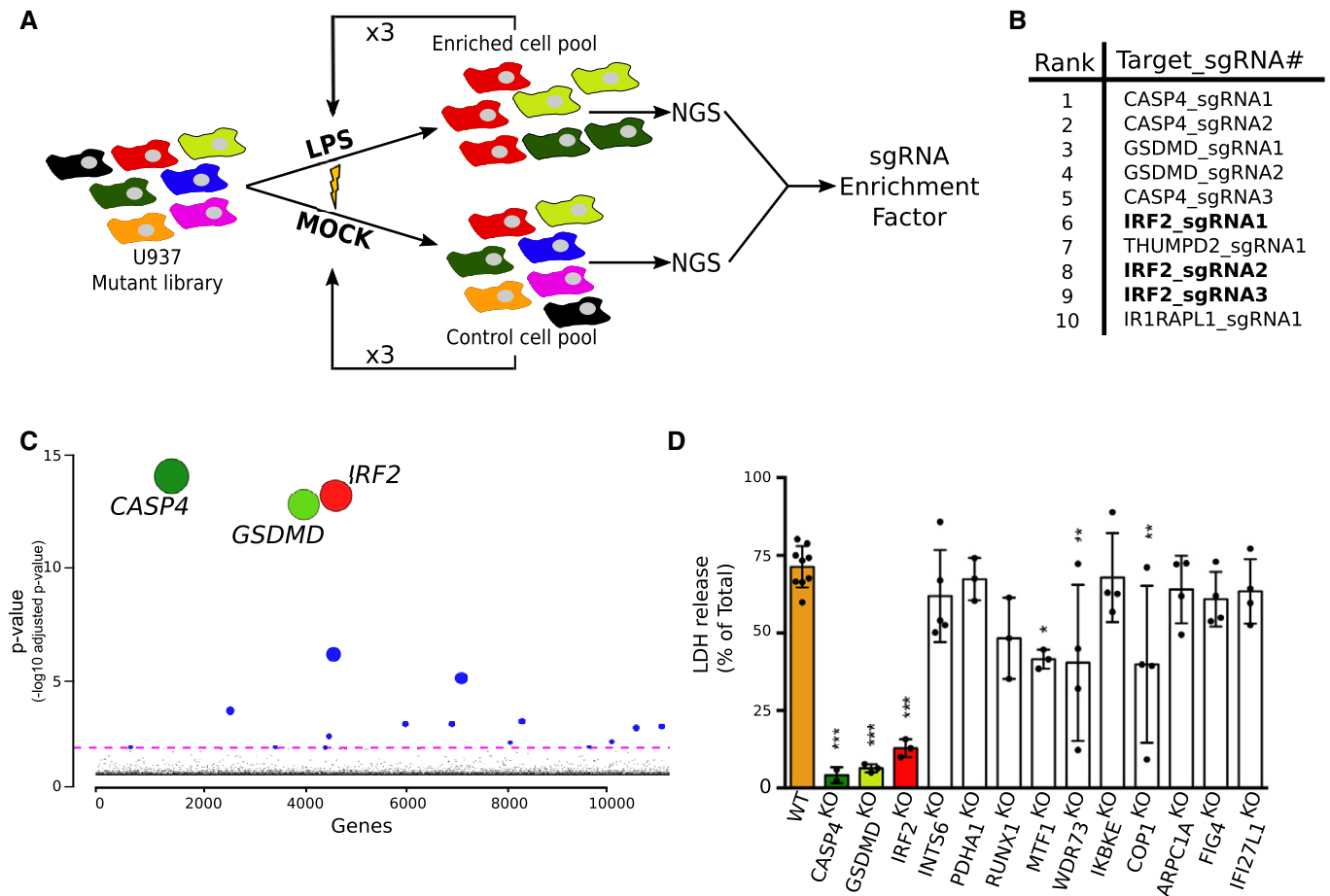


Figure 1. A genome-wide CRISPR/Cas9 screen identifies IRF2, gasdermin D, and caspase-4 as the three main players in LPS sensing.

- A** A genome-wide CRISPR/Cas9 screen based on LPS electroporation was performed in U937 cells. Four successive electroporation rounds were performed. DNA was extracted from surviving cells, and next-generation sequencing (NGS) was performed to calculate the sgRNA enrichment factor.
- B** The 10 most enriched sgRNA in the LPS-electroporated samples are shown.
- C** Graphical representation of the screen results with each gene identified in the output libraries (10,750) represented on the x-axis and the corresponding adjusted *P*-value on the y-axis. Statistical analysis was performed using the Wald test. The colored line represents the 0.05 *P*-value threshold. The size of the circle is inversely proportional to the *P*-value.
- D** U937 cell lines were knock-out using CRISPR/Cas9, and cell death was quantified by LDH release assay 4 h after LPS electroporation. Each dot represents the average of three technical LDH replicates; means and SD of 3–9 independent experiments are shown. One-way ANOVA with Dunnett's multiple comparisons test was performed. Adjusted *P*-value is shown (from left to right ****P* < 0.001, ****P* < 0.001, ****P* < 0.001, *P* = 0.84, *P* = 1, *P* = 0.092, **P* = 0.012, ***P* = 0.0026, *P* = 1, ***P* = 0.0022, *P* = 0.98, *P* = 0.82, *P* = 0.97).

Data information: (A–C) Experiment was conducted once in quadruplicate. *COP1* is also known as *RFWD2*. Source data are available online for this figure.

not observe substantial defects in apoptosis or necrosis kinetics (Fig 2F). Altogether, these experiments demonstrate that, among IRF family members, IRF2 specifically controls pyroptosis in response to cytosolic LPS in U937 monocytes.

IRF2 regulates Caspase-4 level

IRF2 is a transcription factor described to act as transcriptional activator and repressor [40,41]. To understand the mechanisms by which IRF2 controls pyroptosis, we performed transcriptome analysis of wild-type (WT) and *IRF2*^{KO} U937 cells, as well as *IRF2*^{KO} U937 cells reconstituted with *IRF2* (Fig 3A–C). Twenty-four genes (Table EV2) were significantly down-regulated (fold change < 0.5)

in *IRF2*-deficient cells compared to WT cells and significantly up-regulated (fold change > 2) upon reconstitution of *IRF2* expression (Fig 3B). Interestingly, expression of three genes (*CASP1*, *CASP4*, and *CARD16*) from the inflammatory caspase locus [42] was positively regulated by *IRF2* (Fig 3A and C). We did not observe any regulation of *GSDMD* by *IRF2*, either at the transcript level (Fig 3C) or at the protein level (Fig EV3A). To determine whether *IRF2* directly regulated expression of genes in the inflammatory caspase locus, we analyzed *IRF2* chromatin immunoprecipitation coupled to high-throughput sequencing (ChIP-seq) in primary human monocytes [43]. We identified peaks of *IRF2* binding on the promoters of both *CASP4* and *CASP1* genes (Fig 3D), suggesting that *IRF2* directly regulates *CASP1* and *CASP4* expression level.

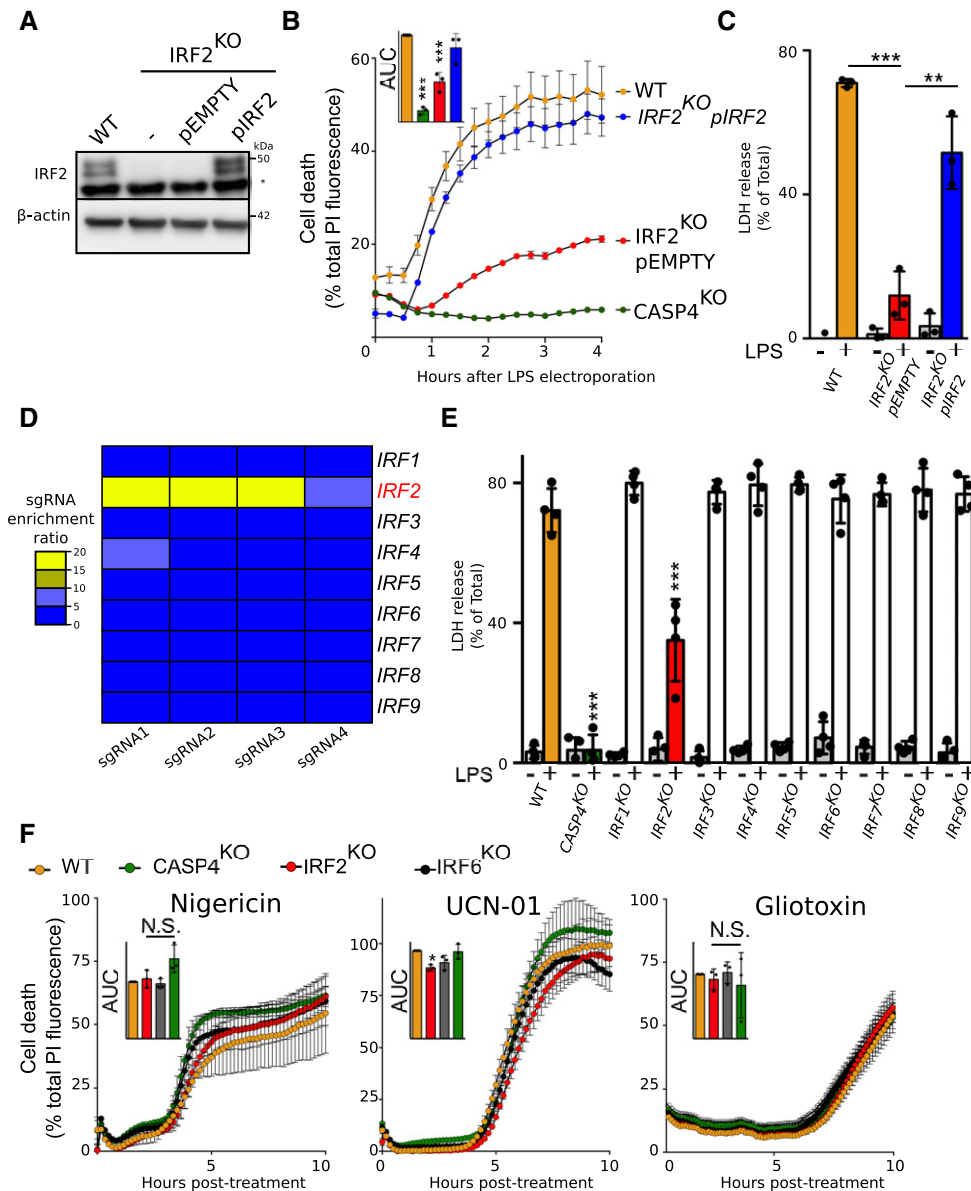


Figure 2. IRF2 is specifically required for caspase-4-mediated cell death.

U937 cell lines were generated using CRISPR/Cas9.

- A IRF2 and β -actin protein levels were assessed in the lysate of the indicated U937 cells by Western blotting analysis. A non-specific band (*) is observed in the IRF2 Western blot. One experiment representative of three experiments is shown.
- B Cell death induced by LPS electroporation or the indicated treatment was quantified in real time by measuring propidium iodide (PI) incorporation/fluorescence every 15 min. Cell death was normalized using untreated and TX-100-treated cells. The kinetics of one representative experiment and the areas under the curve (AUC) (normalized to the WT AUC) of three independent experiments are shown. Each point represents the mean of a biological triplicate of one experiment; the bar represents the mean \pm SD of three independent experiments.
- C Cell death was measured by LDH release assay 4 h after LPS electroporation. Each dot corresponds to the LDH triplicate of one experiment; the bar represents the mean \pm SD of four independent experiments.
- D Heat map representation of the enrichment factor for the 4 sgRNA targeting each IRF in the genome-wide screen.
- E Cell death was measured by LDH release assay 4 h after LPS electroporation. Each dot corresponds to the LDH triplicate of one experiment; the bar represents the mean \pm SD of three independent experiments.
- F Cell death was quantified by measuring PI incorporation/fluorescence every 15 min after treatment with nigericin, UCN-01, or gliotoxin. The kinetics of one representative experiment and the areas under the curve (AUC) (normalized to the WT AUC) of three independent experiments are shown. Each point represents the mean of a biological triplicate of one experiment; the bar represents the mean \pm SD of three independent experiments.

Data information: (B, E and F) One-way ANOVA with Dunnett's multiple comparisons test was performed. (B-WT vs. CASP4^{KO}: *** P < 0.0001, WT vs. IRF2^{KO} pEMPTY: *** P = 0.0004, WT vs. IRF2^{KO} pIRF2: P = 0.11; E-left to right *** P < 0.0001; P = 0.36; *** P < 0.0001; P = 0.78; P = 0.43; P = 0.42; P = 0.98; P = 0.87; P = 0.68; P = 0.86; F- left to right, AUC Nigericin, P = 0.95, P = 0.98, P = 0.027; AUC-UCN-01, P = 0.012; P = 0.066; P = 0.99; AUC gliotoxin, P = 0.97, P = 1, P = 0.79). (C) One-way ANOVA with Sidak's multiple comparisons test was performed. (WT vs. IRF2^{KO} pEMPTY: *** P = 0.0001, IRF2^{KO} pEMPTY vs. IRF2^{KO} pIRF2: ** P = 0.0014).

Source data are available online for this figure.

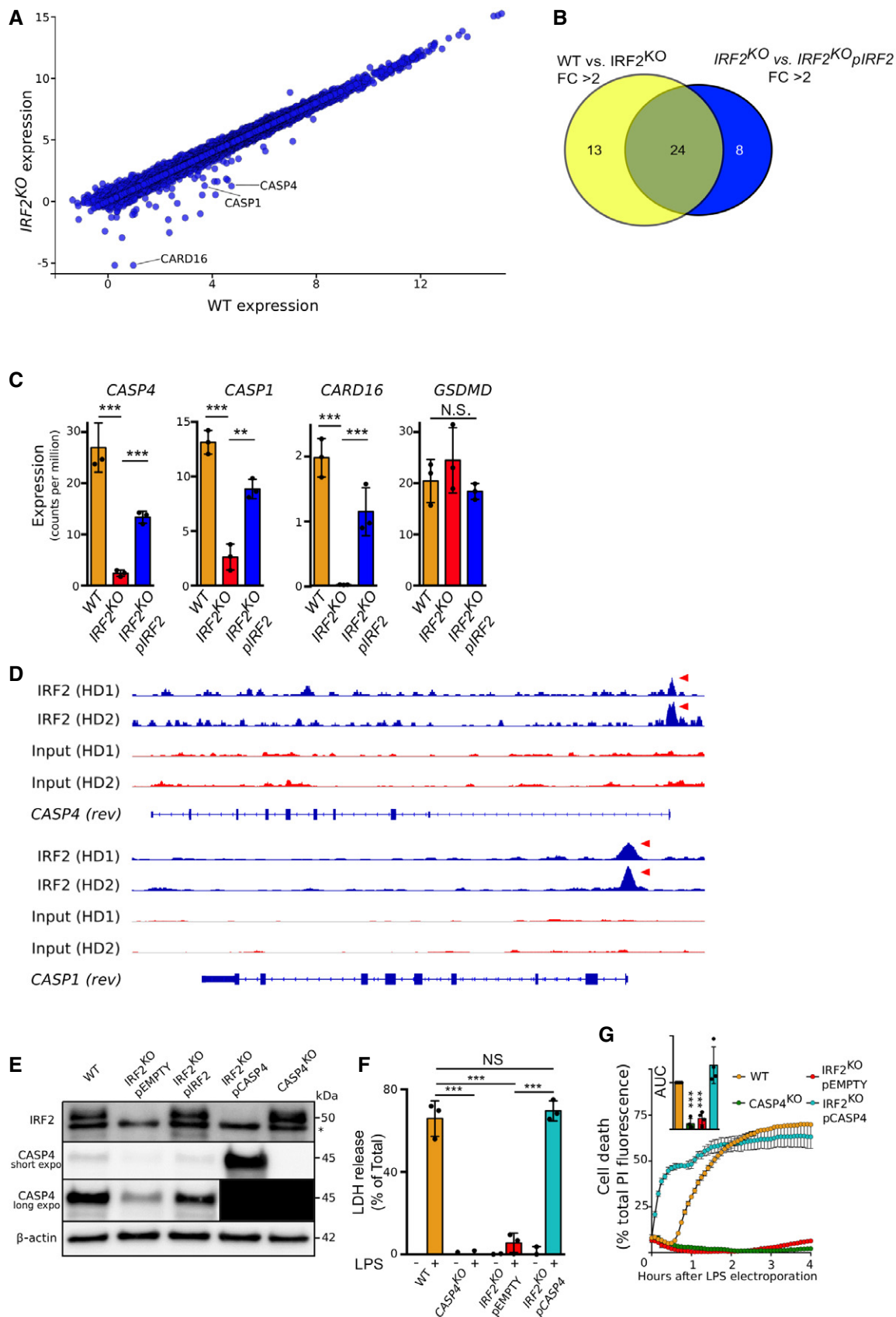


Figure 3.

Figure 3. IRF2 regulates CASP4 transcript levels.

- A mRNA transcript levels in U937 cells WT vs. IRF2^{KO} cells were quantified by RNA-seq.
- B Venn diagram showing the number of genes with a transcript level fold change (FC) greater than 2 in U937 cells WT vs. IRF2^{KO} cells (yellow) and greater than 2 in IRF2^{KO} vs. IRF2^{KO} pIRF2 (Blue).
- C CASP4, CASP1, CARD16, and GSDMD transcript levels were quantified by RNA-seq in the indicated U937 cell lines.
- D Chromatin immunoprecipitation sequencing (ChIP-seq) in primary human monocytes from two healthy donors (HD) for IRF2 binding onto CASP1 and CASP4 promoters. Red arrows indicate promoter region with IRF2 binding.
- E IRF2 and CASP4 protein levels were assessed by Western blotting in the indicated cell lines. The asterisk indicates a non-specific band. For the long exposure of the CASP4 Western blot, the 2 left lanes were covered during revelation to prevent signal bleed through and were blacked out for representation purposes.
- F, G Cell death was quantified by (F) LDH release assay 4 h after LPS electroporation or (G) by measuring propidium iodide (PI) incorporation/fluorescence every 5 min. Cell death was normalized using untreated and TX-100-treated cells. The kinetics of one representative experiment and the areas under the curve (AUC) (normalized to the WT AUC) of four independent experiments are shown. Each point represents the mean of a biological triplicate of one experiment; the bar represents the mean ± SD of four independent experiments.

Data information: (A–C) One experiment performed with three biological replicates. (C) Each point represents the transcript count per million in one biological replicate; the bar represents the mean ± SD of the three replicates. Unpaired *t*-tests were performed. WT vs. IRF2^{KO} *P* = 0.0009, 0.0003, 0.0003, 0.41; IRF2^{KO} vs. IRF2^{KO} pIRF2 *P* = 0.0001, 0.0019, 0.0063, 0.18, for CASP4, CASP1, CARD16, and GSDMD, respectively. (E) Data are representative of three independent experiments. (F) Each dot corresponds to the LDH triplicate of one experiment; the bar represents the mean ± SD of three independent experiments. One-way ANOVA with Sidak's multiple comparisons test was performed. (WT vs. CASP4^{KO}, WT vs. IRF2^{KO} pEMPTY, IRF2^{KO} pEMPTY vs. IRF2^{KO} pCASP4 all ****P* < 0.0001, WT vs. IRF2^{KO} pCASP4: *P* = 0.90 NS: not significant) (G) One-way ANOVA with Dunnett's multiple comparisons test was performed. (WT vs. CASP4^{KO}: ****P* = 0.0003, WT vs. IRF2^{KO}: ****P* = 0.0008, WT vs. IRF2^{KO} pCASP4: *P* = 0.078).

Source data are available online for this figure.

The strong and specific regulation of CASP4 mRNA levels by IRF2 (Fig 3C) suggested that IRF2 might control pyroptosis through the control of CASP4 expression. We thus assessed caspase-4 protein levels in WT, IRF2^{KO}, and pIRF2-reconstituted cell lines by Western blotting. In line with the transcriptomic data, we observed a strong decrease in caspase-4 (Fig 3E) and caspase-1 (Fig EV3B) protein levels in IRF2^{KO} U937 cells, which could be corrected upon IRF2 reconstitution. As expected, the reduction in caspase-1 levels was associated with decreased IL-1β release upon activation of the NLRP3 inflammasome with LPS + nigericin (Fig EV3C).

Because of the direct link between IRF2 activity and caspase-4 expression, we next tested whether expressing CASP4 under a constitutive promoter (Fig 3E–G) could restore pyroptosis in IRF2^{KO} cells. Indeed, constitutive expression of CASP4 led to strong LDH release upon LPS transfection in IRF2^{KO} cells (Fig 3F). Interestingly, overexpression of CASP4 in IRF2^{KO} cells decreased the delay between LPS electroporation and membrane permeabilization as visualized by PI fluorescence, indicating that caspase-4 levels control the cell death response kinetics (Fig 3G). Altogether, these results demonstrate that IRF2 positively regulates caspase-4 levels in U937 monocytes, which is required for these cells to trigger pyroptosis in response to LPS electroporation.

IFN-γ treatment induces IRF1 to cooperate with IRF2 to regulate CASP4 transcript level and LPS-mediated pyroptosis

Inflammasome activation can be modulated by the surrounding inflammatory milieu. We therefore assessed the role of IRF2 in LPS-induced pyroptosis in the presence of IFN-γ, a prominent anti-bacterial cytokine [44]. Surprisingly, IFN-γ treatment restored pyroptosis in IRF2-deficient cells to levels observed in WT cells (Fig 4A). Since numerous IRFs are IFN-inducible and share similar binding sites [45], we hypothesized that other IRFs could compensate for the absence of IRF2 after IFN-γ treatment. To test this hypothesis, we generated cell lines double-knock-out (DKO) for IRF2 and each individual IRF (Appendix Table S1). Remarkably, the

IRF1/IRF2^{DKO} cell line was resistant to LPS electroporation-induced pyroptosis even in the presence of IFN-γ, while none of the other cell lines showed any substantial difference with WT cells after IFN-γ treatment (Fig 4B).

We further validated the redundant role of IRF1 and IRF2 in the presence of IFN-γ by monitoring LPS-induced cell death in real time using PI incorporation. We found that while IRF2 deficiency alone was insufficient to prevent LPS-mediated pyroptosis after IFN-γ treatment, double-knock-out cells were largely resistant to cell death (Fig 4C). By blotting for caspase-4 protein levels in IRF2^{KO} and IRF1/IRF2^{DKO} cell lines, we observed that in the presence of IFN-γ, expression of caspase-4 increased in IRF2^{KO} cells and that this increase was dependent on IRF1 (Fig 4D). In contrast, we did not observe any substantial induction of caspase-4 protein in the presence of either Pam3CSK4, a TLR2 agonist, or extracellular LPS (Appendix Fig S2). Although we cannot exclude that other IRF-1-induced genes [30,34,46,47] may participate in restoring the sensitivity of IRF2-deficient cells to electroporated LPS (see GBP1 in Appendix Fig S3), our data suggest that the dual regulation of caspase-4 levels by IRF1 and IRF2 contributes to cytosolic LPS-mediated pyroptosis in the presence of IFN-γ.

IRF2 controls, in a partially redundant manner with IRF1, caspase-4-mediated responses during infection in macrophages

To obtain robust inflammasome activation following *E. coli* and *F. novicida* infection, U937 monocytes must first be differentiated into macrophages using PMA and priming with IFN-γ [30]. Since IL-1β secretion upon cytosolic LPS delivery is mediated by the NLRP3 inflammasome downstream of the caspase-4-gasdermin D cascade [16], Pam3CSK4 was used to induce proIL-1β and prime the NLRP3 inflammasome. In IFN-γ-primed, PMA-differentiated U937 macrophages, as described above, the presence of IRF1 compensated IRF2 deficiency in regulating LDH release and IL-1β release upon cytosolic delivery of LPS (Fig 5A and B). U937 macrophages deficient in both IRF1 and IRF2 displayed a profound

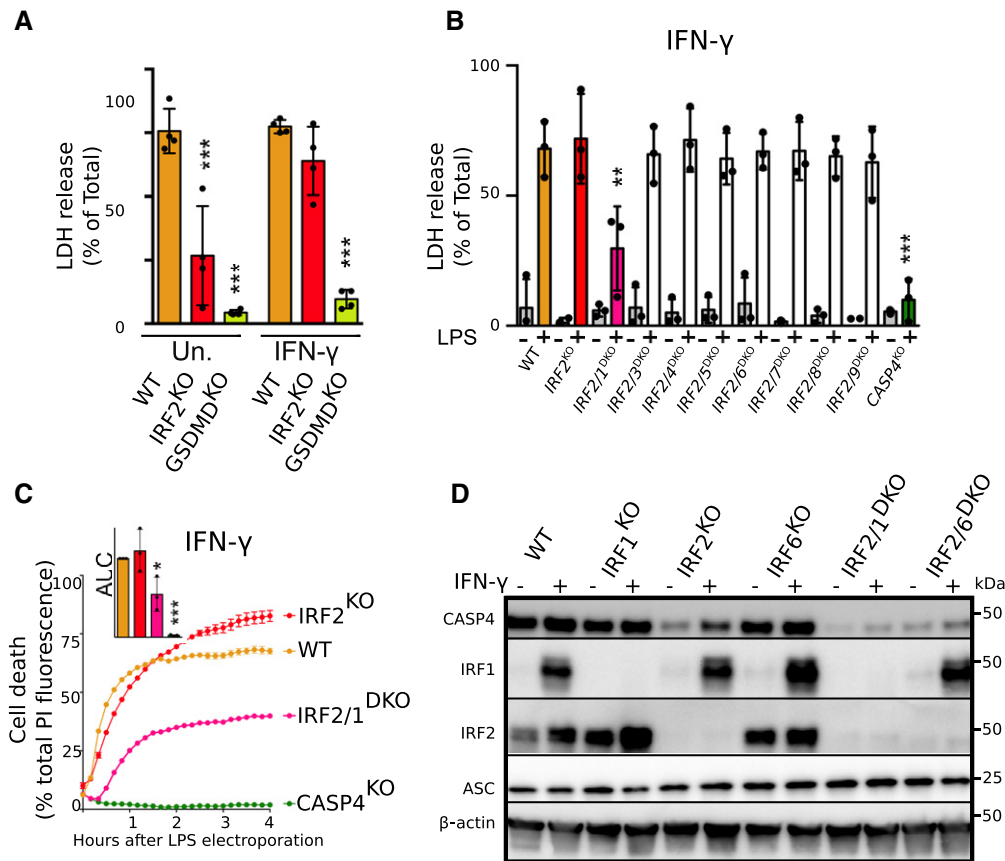


Figure 4. IFN- γ treatment induces IRF1 to redundantly act with IRF2 to regulate caspase-4 levels and LPS-mediated pyroptosis.

A–C Cell death was assessed (A, B) by measuring LDH release 4 h after LPS electroporation or (C) by measuring propidium iodide (PI) incorporation/fluorescence every 10 min in the indicated U937 cell lines primed (A–as indicated, B, C–all samples) or not with IFN- γ . (C) Cell death was normalized using untreated and TX-100-treated cells. One real-time cell death experiment (mean and SD of triplicate) representative of three independent experiments is shown. The areas under the curve (AUC) (normalized to the WT AUC) of three independent experiments are shown. Each point represents the mean of a triplicate of one experiment; the bar represents the mean (and SD) of the three independent experiments.

D Caspase-4, IRF2, and IRF1 protein levels were assessed in the lysate of the indicated U937 cell lines primed or not with IFN- γ . Data are representative of three independent experiments.

Data information: (A,B) Each dot corresponds to the mean of LDH triplicate of one experiment; the bar represents the mean \pm SD of three (B) to four (A) independent experiments. (A): One-way ANOVA with Sidak's multiple comparisons test was performed (untreated WT vs. IRF2^{KO}: *** P < 0.0001, WT vs. GSDMD^{KO}: *** P < 0.0001; IFN- γ -treated WT vs. IRF2^{KO}: P = 0.3, WT vs. GSDMD^{KO}: *** P < 0.0001). (B) One-way ANOVA with Dunnett's multiple comparisons test was performed (All P -values = 1 except WT vs. IRF1/2^{DKO}: ** P = 0.0048 and WT vs. CASP4^{KO}: *** P < 0.0001). (C) One-way ANOVA with Dunnett's multiple comparisons test was performed (WT vs. IRF2^{KO}: P = 0.84, WT vs. IRF1/2^{DKO}: * P = 0.03, WT vs. CASP4^{KO}: *** P = 0.0004).

Source data are available online for this figure.

decrease in LPS-mediated cytotoxicity and IL-1 β release (Fig 5A and B).

We then investigated the role of IRF1 and IRF2 in controlling caspase-4-mediated responses during infection. We used *F. novicida* to infect cells, as it is known to activate caspase-4 in human macrophages [30]. As previously described for murine macrophages [34], mutation of *IRF1* highly delayed cell death in IFN- γ -primed U937 macrophages that were infected with *F. novicida* (Fig 5C), likely through the regulation of guanylate binding proteins (GBPs) [30,34] (Appendix Fig S3). Mutation of *IRF2* alone had no significant effect; however, in *IRF1*^{KO} cells, *IRF2* deletion delayed *F. novicida*-mediated cell death and fully abolished caspase-4-dependent cell death (Fig 5C). Of note, cell death kinetics were substantially slower in *IRF1/2*^{DKO} cells than in *CASP4*^{KO} cells suggesting that IRF1 and IRF2

control both non-canonical and canonical inflammasome-mediated cell death during *F. novicida* infection. In addition to regulating cell death, IRF1 and IRF2 deficiency also affected cytokine release after *F. novicida* infection. In particular, single inactivation of either *IRF1* or *IRF2* deeply and significantly dampened IL-1 β release (Fig 5D) while TNF levels were largely consistent across all genotypes (Fig 5E). Similar results were observed upon *E. coli* infection (Fig 5F–H), although the contribution of caspase-4 to cell death and IL-1 β release was only partial in this model. Altogether, these results demonstrate that, during infection of IFN- γ -primed U937 macrophages, IRF2 acts in a partially redundant manner with IRF1 to control inflammasome responses. This action likely occurs through the regulation of caspase-4 levels, as well as other innate immune proteins (Appendix Fig S2 and S3).

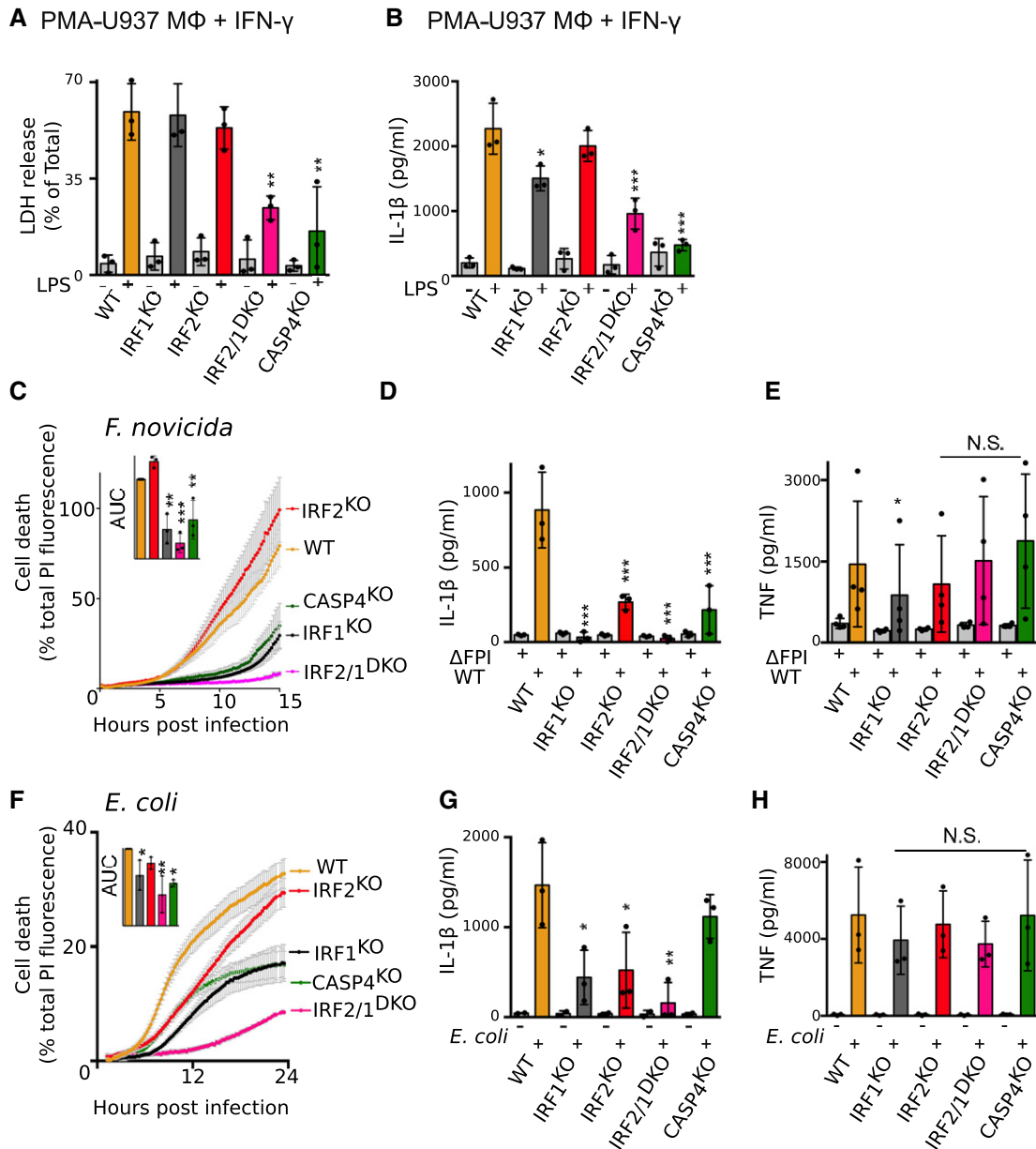


Figure 5. IRF1 cooperates with IRF2 to regulate non-canonical inflammasome activation in PMA-differentiated macrophages.

U937 cell lines were differentiated with PMA and primed with IFN- γ .

A Cell death was quantified by LDH assay 2 h after LPS electroporation.

B Cells were primed with Pam3CSK4. IL-1 β levels were assessed by ELISA 4 h after LPS electroporation.

C Cell death was quantified by measuring propidium iodide (PI) incorporation/fluorescence every 5 min after infection with *F. novicida* or (F) *E. coli*. Cell death was normalized using untreated and TX-100-treated cells. One real-time cell death experiment (mean and SD of triplicate) representative of three independent experiments is shown. The areas under the curve (AUC) (normalized to the WT AUC) of three independent experiments are shown. Each point represents the mean of a triplicate of one experiment; the bar represents the mean (and SD) of the three independent experiments.

(D–H) (D, G) IL-1 β and (E, H) TNF levels were assessed by ELISA 6 h after WT or Δ FPI mutant *F. novicida* (D, E) or *E. coli* (G, H) infection.

Data information: (A, B) Each dot corresponds to the mean of LDH triplicate of one experiment; the bar represents the mean \pm SD of three independent experiments. (D–E, G–H) Each dot corresponds to the mean of biological triplicates of one experiment, the bar represents the mean \pm SD of three (D, G, H) to four (E) independent experiments. (A–H) One-way ANOVA with Dunnett's multiple comparisons test was performed. (A) WT vs. IRF1/2^{KO} $^{**}P = 0.0084$, WT vs. CASP4^{KO} $^{**}P = 0.0019$ (B) WT vs. IRF1^{KO} $^{*}P = 0.012$, WT vs. IRF1/2^{KO} $^{***}P = 0.0003$, WT vs. CASP4^{KO} $^{***}P < 0.0001$ (C) (WT vs. IRF2^{KO}: $P = 0.26$, WT vs. IRF1^{KO}: $^{**}P = 0.0015$, WT vs. IRF1/2^{DKO}: $^{***}P = 0.0002$, WT vs. CASP4^{KO}: $^{**}P = 0.0067$). (D) (WT vs. IRF2^{KO}: $^{***}P = 0.001$, WT vs. IRF1^{KO}: $^{***}P < 0.0001$, WT vs. IRF1/2^{DKO}: $^{***}P < 0.0001$, WT vs. CASP4^{KO}: $^{***}P = 0.0005$). (E) (WT vs. IRF2^{KO}: $P = 0.045$, WT vs. IRF1^{KO}: $^{*}P = 0.19$, WT vs. IRF1/2^{DKO}: $P = 1$, WT vs. CASP4^{KO}: $P = 0.57$). (G) (WT vs. IRF2^{KO}: $^{*}P = 0.016$, WT vs. IRF1^{KO}: $^{*}P = 0.024$, WT vs. IRF1/2^{DKO}: $^{**}P = 0.0032$, WT vs. CASP4^{KO}: $P = 0.57$). (F) WT vs. IRF1^{KO} $^{*}P = 0.045$, WT vs. IRF1/2^{DKO} $^{**}P = 0.0017$, WT vs. CASP4^{KO} $^{*}P = 0.0107$ (H) (WT vs. IRF2^{KO}: $P = 0.86$, WT vs. IRF1^{KO}: $P = 1$, WT vs. IRF1/2^{DKO}: $P = 0.79$, WT vs. CASP4^{KO}: $P = 1$).

Source data are available online for this figure.

IRF2 controls caspase-4 levels in human iPSC-derived macrophages

To validate our findings in a more relevant cellular system, we deleted *IRF2* in human induced pluripotent cells (iPSC). Gene deletion was confirmed at the DNA level by sequencing (Appendix Fig S4) and at the protein level in iPSC-derived macrophages (Fig 6A). Corroborating observations made in U937 cells, deletion of *IRF2* in iPSC-derived macrophages led to a strong reduction in caspase-4 protein levels (Fig 6A). At odds with the results obtained in U937 cells, we did not observe any impact of *IRF2* deletion on caspase-1 protein levels in iPSC-derived macrophages, possibly reflecting interindividual variability. In line with the role of IRF2 as a transcription factor, *CASP4* transcript levels were also strongly and significantly reduced in the two *IRF2* knock-out iPSC-derived macrophage clones. *NLRP3*, *ASC*, and *CASP1* did not display any reduction in their transcript levels (Fig 6B). Altogether, these results demonstrate that in human cells, IRF2 is a key regulator of caspase-4 levels.

Discussion

Here, we describe an unbiased, genome-wide screen used to identify genes involved in non-canonical inflammasome activation in human cells. We found that three genes—encoding caspase-4, gasdermin D, and IRF2—were significantly associated with non-canonical inflammasome activation and therefore represent the core pathway controlling cytosolic LPS-mediated cell death in human cells. This

work not only supports the role of caspase-4 as the direct LPS receptor and effector of the non-canonical inflammasome complex [8], but also identifies IRF2 as a novel factor regulating caspase-4 expression levels and non-canonical inflammasome activation in human cells. Further, this screen stresses the unusual simplicity of this signaling complex, particularly when compared to the large number of proteins involved in extracellular LPS sensing by TLR4, and in its downstream signal transduction pathway [48].

The remaining 15 significant hits identified in this screen were not investigated in the present study. These genes likely include both minor contributors and false positives. We cannot rule out the existence of other regulators that may have been missed in the screen either due to redundancy or to our experimental system. For example, U937 cells may not fully model primary monocytes in terms of expression or regulation. Furthermore, electroporation of LPS was required to trigger a robust and reproducible cell death, but likely prevented the identification of host molecules required for LPS trafficking from the extracellular environment to the cytosol, or for the extraction of lipid A from its membrane environment (e.g. outer membrane vesicles—OMVs). Indeed, we and others have previously identified the GBPs as co-factors regulating non-canonical inflammasome activation in response to Gram-negative infection, OMV internalization, or LPS transfection [30,46,47,49]. These proteins were not identified in the screen.

Expression of caspase-11 in mouse cells is highly inducible by multiple pro-inflammatory stimuli including TLR ligands and IFNs [27]. Conversely, caspase-4 is constitutively expressed in human monocytes and macrophages [28,29,50], which correlates with the

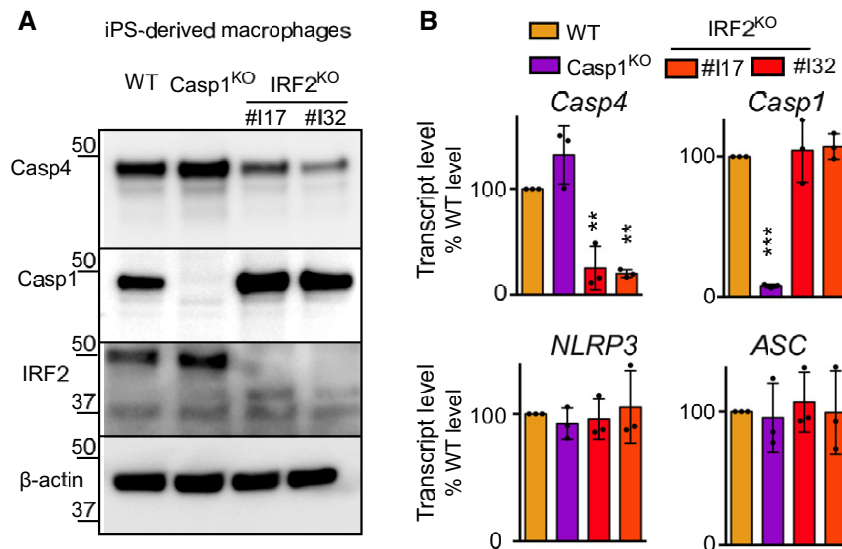


Figure 6. IRF2 controls caspase-4 levels in human induced pluripotent stem cell (iPSC)-derived macrophages.

A, B Macrophages were derived from human iPSC clones knock-out for the indicated genes. Two clones were selected for *IRF2*^{KO} cells. (A) Caspase-4, caspase-1, IRF2, and β -actin protein levels were assessed by Western blotting analysis. One experiment representative of two independent experiments is shown. (B) The indicated mRNA levels were quantified by qRT-PCR normalized to β -actin mRNA levels and expressed as fold change compared to WT levels. Each dot represents the average of a technical RT-PCR triplicate from one experiment; the bar represents the mean of three independent experiments. One-way ANOVA with Dunnett's multiple comparisons test was performed (WT vs. *IRF2*^{KO} #17 ***P* = 0.0020; WT vs. *IRF2*^{KO} #32 ***P* = 0.0013 for *CASP4* transcript. WT vs. *CASP1*^{KO} ****P* < 0.0001 for *CASP1* transcript levels).

Source data are available online for this figure.

high sensitivity of humans to LPS compared to mice [6,51]. Our results demonstrate that IRF2 is required for this constitutive expression and is responsible for the sensitivity of human monocytes to LPS-mediated pyroptosis. Accordingly, IRF2 is constitutively expressed [52] in monocytes and acts as a transcriptional activator of caspase-4 expression. In contrast, IRF-1 expression is strongly inducible by IFN- γ and compensates *IRF-2* deficiency in IFN- γ -primed cells. This result is consistent with the ability of IRF-1 and IRF-2 to bind to the same recognition site [53] and suggests that in the presence of IFN- γ , IRF1 and IRF2 ensure a robust and possibly redundant control of caspase-4 expression. Interestingly, this regulatory mechanism is not limited to the *CASP4* gene; in epithelial cells, TLR3 expression is positively regulated by IRF2 at steady state, while treatment with IFN leads to IRF1-dependent control [41]. This regulation exemplifies the recurring theme of redundancy in innate immunity [54], which is thought to contribute to the robustness of the innate immune system in humans. The redundant mechanisms controlling caspase-4 expression in the presence of IFN- γ likely ensure the efficiency of cytosolic LPS detection during infection. Another potentially redundant player of this system is caspase-5, a poorly characterized human inflammatory caspase detecting LPS in the cytosol. Yet, caspase-5 was not expressed in our U937 experimental system—even in the presence of IFN- γ —and we were thus unable to investigate the potential role of IRF1/2 in regulating caspase-5 levels.

IRF2^{-/-} mice exhibit resistance to LPS-induced lethality [55]. This resistance had been associated with a greater number of apoptotic Kupffer cells in IRF2^{-/-} mice than in WT mice upon LPS injection. Yet, while this manuscript was under review, IRF2 was demonstrated to regulate gasdermin D level in murine macrophage through direct binding of the *GSDMD* promoter region [56]. The study also found that IRF1 could compensate for the absence of IRF2 in controlling gasdermin D levels, similar to what we found for IRF1 regulation of caspase-4 in human cells. Interestingly, IRF2 in that study was found to control gasdermin D but not caspase-4 levels in the human EA.hy926 cell line [57]. In contrast, we did not observe any substantial regulation of GSDMD levels by IRF1/2 in U937 cells at steady state (Fig EV3A and Appendix Fig S2). However, we observed an IFN- γ -mediated increase in GSDMD level that was abolished in IRF1/2^{DKO} cells (Appendix Fig S2). This result strongly suggests a role of IRF1 (and potentially IRF2) in the regulation of human GSDMD. Further studies are needed to better characterize the regulation of GSDMD by IFN- γ and to understand its relevance in the context of cell death and cytokine secretion. At this stage, it is unclear whether the differences observed at steady state between the different human cell lines reflect interindividual variations in the promoter regions of inflammasome genes or whether IRF2 controls different subsets of genes in different cell types. Altogether, these studies strongly demonstrate that IRF2 has a conserved role in mice and humans to control inflammasome genes.

Interestingly, IRF2 expression is differentially regulated in human individuals in response to LPS [43], suggesting that single nucleotide polymorphisms (SNPs) affecting IRF2 levels might control interindividual susceptibility to Gram-negative bacteria and septic shock. Similarly, common variants in *IRF5* modulate the antimicrobial responses of human macrophages [58,59], indicating that the polymorphisms in the various *IRF* genes may be an important driver of the interindividual differences in susceptibility to bacterial infections. Recently, IRF-1 and IRF-8 were demonstrated to regulate Gbps and

Naips expression in mice [34,35]. Collectively, these data demonstrate the emerging role of IRFs as central regulators of inflammatory accessory proteins, sensors, and effectors in mice and humans.

Materials and Methods

Genome-wide CRISPR/cas9 screen

The Brunello library obtained from Addgene (ref# 73178) is made of 76,441 sgRNAs targeting 19,114 human genes and 1,000 non-targeting control sgRNAs, all cloned in lentiGuide-Puro (Addgene ref# 52963). A clonal population of U937 Cas9⁺ was infected with a virus library titrated in order to achieve an MOI of 0.5 and a 390-fold coverage for each sgRNA. Starting at 3 days post-transduction, cells were treated with puromycin at 2 mg/ml for 12 days. Four replicates of 4 × 10⁶ cells were then electroporated with 10 μ g of *F. novicida* LPS or mock-electroporated using the Neon electroporator (1 pulse of 1.3 KV and 30 ms width). This operation was repeated three more times with 4 days of recovery between each electroporation. DNA was extracted using a kit from Macherey-Nagel. sgRNA containing regions were amplified by nested PCR using the following 1st set of primers: Fwd 5'-AATGGACTATCATATGCTTACCGTAACTTGAAAAGTATTTCCG-3', Rev 5'-CTTTAGTTTTGATGTCTGTTGCTATTATGTCTACTATTCTTTCC-3' and 2nd set of primers: Fwd 5'-PRIMER FUSION+BARCODE+TCTTGTGGAAAGGACGAAACACCG-3', Rev 5'-PRIMER FUSION+TCTACTATTCTTCCCTGCACTGT-3'. For the mock-transfected samples, 56 PCRs were performed using the first set of primers (1 μ g of DNA per reaction in a 50 μ l volume). These samples were then pooled, and 5 μ l of this product was used as a template for 24 additional PCRs (using primer set 2 in a 50 μ l final volume). For the LPS-transfected samples, 36 PCRs were performed using primer set 1 (1 μ g of DNA per reaction in a 50 μ l volume). Again, these samples were pooled, and 5 μ l of this product was used to run 16 PCRs with primer set 2. The barcodes were used to discriminate different samples in the same run of sequencing. The primer fusion was required for performing next-generation sequencing on the Ion Proton system (Thermo Fisher). The experimental depth of sequencing was at least 15 million sequences reads per sample. Raw data were obtained as fastq files. Low-quality sequences and sequences with < 30 reads were removed, and primers were trimmed. The sequences obtained were aligned against the reference library of sgRNA. sgRNA enrichment factor was determined by the ratio between the number of reads for a given sgRNA in LPS-treated and control sample. Statistical analysis was performed using the R DESeq2 package. First, counts were normalized to account for differences in sequencing depth between sgRNAs; that is, each sgRNA raw count was divided by its own size factor. Then, the normalized data were tested for differential expression between the LPS-electroporated and the mock samples using Wald significance tests. The sgRNA enrichment factor was calculated by dividing the number of normalized reads for sgRNA in LPS treatment sample by the number of normalized reads for sgRNA in mock sample.

Cell culture

The human myeloid cell line U937 (obtained from CelluloNet) was grown in RPMI 1640 media with glutaMAX-I (#61870-010)

supplemented with 10% (vol/vol) FBS, 100 IU/ml penicillin, and 100 µg/ml streptomycin (all from Thermo Fisher Scientific). When indicated, U937 cells were treated with 100 ng/ml of phorbol 12-myristate 13-acetate (PMA; InvivoGen) for 48 h to trigger differentiation into macrophages.

iPSC generation and differentiation

NCRM-1 iPSC (RRID:CVCL_1E71), available at the NIMH Repository and Genomics Resource, were matured and differentiated into macrophages (iPSC-MC) in the absence of feeding layers and in serum-free conditions as previously described [60]. Briefly, cells were cultured in colonies in StemFlex™ medium (Thermo Fisher Scientific) and mechanically dissociated using TrypLE (Thermo Fisher Scientific) to obtain single cell suspensions. For the generation of embryoid bodies (EBs), 10^4 cells were spun down and cultured in the presence of 1 mM Rock inhibitor (Y27632; Calbiochem), 50 ng/ml BMP-4 (Peprotech EC Ltd.), 20 ng/ml SCF (Miltenyi Biotec Ltd), and 50 ng/ml VEGF. After 4 days, 70 EBs were seeded in 10-cm² extra-adherent CellBIND plates (Corning) and cultured in X-VIVOTM 15 serum-free hematopoietic cell medium (Lonza) in the presence of human 100 ng/µl IL-3 (R&D) and 100 ng/µl M-CSF (Thermo Fisher Scientific) to induce myeloid differentiation. Cells were harvested every 5 days and further matured in X-VIVOTM 15 media in the presence of M-CSF only during 4 days for terminal macrophage differentiation.

CRISPR/Cas9

All U937 knock-out cell lines generated by CRISPR in this study were generated in a Cas9-expressing U937 clone obtained by transduction with the plasmid LentiCas9-Blast (from Feng Zhang; Addgene plasmid # 52962) followed by blasticidin selection and clonal isolation using the limit dilution method. A clone strongly expressing Cas9 was selected based on Western blot analysis using anti-Cas9 antibody (Millipore; # MAC133; 1:1,000 dilution). sgRNAs for all the genes targeted (Appendix Table S2) were cloned into the pKLV-U6gRNA(BbsI)-PGKpuro2ABFP vector (from Kosuke Yusa; Addgene plasmid # 50946). For each gene, two sgRNAs were used. Lentiviral particles were produced in 293T cells using pMD2.G and psPAX2 (from Didier Trono, Addgene plasmids #12259 and #12260), and pKLV-U6gRNA(BbsI)-PGKpuro2ABFP. U937 Cas9⁺ cells were transduced by spinoculation. A polyclonal population was selected using puromycin treatment. Gene invalidation was verified by Western blot analysis, visualization of DNA fragment deletion on agarose gel, or using TIDE software. All knock-out validation details are available in Appendix Table S1.

For generation of *IRF2* NCRM-1 knock-out cells, cells were co-transfected with two pL-CRISPR.SFFV.GFP (from the laboratory Benjamin Ebert; Addgene plasmid #57827) plasmids containing two different sgRNAs targeting exon 7 or 8 of *IRF2*. For generation of caspase-1 NCRM-1 knock-out cells, cells were co-transfected with two px330-P2A-GFP plasmids containing two different sgRNAs targeting exon 1 of *CASP1*. Transfection was performed using Amaxa™ Human Stem Cell Nucleofector™ Kit 2 (Lonza). GFP-positive cells were sorted and grown at low density in Matrigel-coated plates in the presence of 1 mM Rock inhibitor (Y27362; Calbiochem). Single-clone colonies started forming after 4 days of culture,

and when fully grown were amplified and validated by sequencing. Knock-outs were then further validated at the protein level in terminally differentiated macrophages by Western blot.

Complemented cell lines

CASP4 cDNA was obtained from J.Yuan and cloned into a pAIP lentiviral vector (from A. Cimarelli) as previously described [30]. An *IRF2* coding sequence with mutated PAM sites was synthesized (Thermo Fisher) and cloned into pAIP using NotI and XhoI restriction enzymes. Each of these constructs was packaged into a lentivirus, and U937 *IRF2*^{KO} cells were transduced as described above. Seventy-two hours post-transduction, stably transduced cells were selected with 2 µg/ml Puromycin (Sigma-Aldrich) for 10 days.

RNA-seq

RNA was extracted from U937 cell lines, and libraries were prepared using the SENSE mRNA-Seq Library Prep Kit V2 (Lexogen) and sequenced on an Illumina NextSeq500 (75 bp in single end) with at least 20 millions reads per sample. Obtained sequences were trimmed, filtered, and aligned using the Tophat package. Genes with an absolute transcript count inferior to 30 reads in all the libraries were filtered out. Differential expression analysis was performed after normalization using limma-trend (package in R).

ChIP-seq

IRF2 ChIP-Seq raw data were kindly provided by Benjamin Fairfax [43]. Adaptor sequences, low-quality nucleotides with a Phred score below 20, and reads with lengths shorter than 25 nucleotides were removed with the Trimmomatic tool [61]. Trimmed reads were aligned to the GrCH37/Hg18 human genome build with the Bowtie2 tool by using default parameters [62]. Reads mapped with low mapping quality (MAPQ < 10) were discarded with samtools [63]. Duplicated reads were removed with MarkDuplicates from picard tools (<https://broadinstitute.github.io/picard/>). Narrow peak calling was performed with MACS2 [64]. BigWig files were created from MACS2 bedGraph with BEDtools [65]. Results were visualized with Integrative Genomic Viewer (IGV) [66].

Delivery of intracellular LPS

U937 was electroporated with LPS using the Neon® Transfection System (Thermo Fisher Scientific, # MPK10096) according to the manufacturer's protocol (1 pulse of 1.3 kV and 30 ms width). Western blot analyses were performed at 1 h post-electroporation. Cell death assays were performed at 4 h post-electroporation. LPS from *E. coli* O111:B4 (InvivoGen) was used at 5 µg for 5×10^5 cells. LPS from *F. novicida* was kindly provided by Wayne Conlan (National Research Council Canada).

Cytokine release measurement and cell death assay

ELISA kits were from R&D Systems (#DY210, DY201). Quantification of cell death was performed by monitoring LDH release in the supernatant using the Cytotoxicity detection kit (Roche, #11644793001). Cell death was also quantified by monitoring propidium iodide (PI)

incorporation. Briefly, 5×10^4 U937 cells were seeded in black 96 flat-bottom well plates with CO₂-independent medium (Thermo Fisher, #18045054) supplemented with 10% (vol/vol) FBS. PI was added at a final concentration of 5 µg/ml. Fluorescence was measured on a microplate fluorimeter (Tecan). Cell death was normalized by removing PI fluorescence of untreated cells and using the PI fluorescence value of 1% Triton X-100-treated cells as a measure of total cell death (average of the last 4 kinetics points).

Immunoblot analysis

Cells were lysed with RIPA buffer containing Mini EDTA-free Protease Inhibitor Mixture (Roche, #11836170001). Proteins were separated by SDS/PAGE on precast 4–15% acrylamide gels (Bio-Rad, #4561084) and transferred to TransBlot® Turbo™ Midi-size PVDF membranes (Bio-Rad, #1704157). Antibodies used were mouse monoclonal anti-caspase-4 (MBL; clone 4B9; #M029-3; 1:1,000 dilution), rabbit monoclonal anti-caspase-1 (Cell Signaling; #3866; 1:1,000 dilution), rabbit monoclonal anti-IRF1 (Cell Signaling; #8478; 1:1,000 dilution), mouse monoclonal anti-IRF2 (Santa Cruz; #sc-374327; dilution 1:1,000 or sc-101069; dilution 1:1,000), anti-gasdermin D (Cell Signaling, #96458; dilution 1:1,000). As loading control, cell lysates were reprobated with a mouse monoclonal antibody anti-β-actin (clone C4, Millipore; 1:5,000 dilution). Full Western blot images are presented in the raw data source files.

U937 stimulation

To induce apoptotic cell death, cells were treated with either UCN-01, a staurosporine derivative (Sigma; #U6508) at 12.5 mM, or gliotoxin (Enzoflife; #BML-PI129) at 500 ng/ml. For necrosis induction, unprimed U937 cells were treated with Nigericin (Invivogen; #tlr-nig) at 50 µg/ml. When indicated, U937 cells were primed with Pam3CSK4 (Invivogen) at 1 µg/ml for 3 h, or with IFN-γ (Immunotools) at 1000 µg/ml for 16 h before LPS electroporation. For NLRP3 activation, PMA-differentiated macrophages were primed with Pam3CSK4 (Invivogen) at 1 µg/ml for 16 h, followed by 2 h of Nigericin at 30 µg/ml.

Bacterial strains and macrophage infection

F. novicida strain Utah (U112) was grown in tryptic soy broth (Conda) supplemented with 0.1% (w/v) cysteine. *E. coli* J53 strain was grown in Luria broth (Conda). U937 cells were plated at a concentration of 5×10^4 cells in 96-well plates. Prior to infection, U937 cells were treated 48 h with PMA for differentiation into macrophages. Additionally, U937 were stimulated with 1,000 U/ml IFN-γ (Immunotools). Bacteria were added onto macrophages at a multiplicity of infection (MOI) of 100:1 (*F. novicida*) or 10:1 (*E. coli*). The plates were centrifuged for 15 min at $1,000 \times g$ and incubated for 1 h at 37 °C. Next, cells were washed and fresh medium with 10 µg/ml gentamicin (Thermo Fisher Scientific) was added before incubation for the indicated time.

Real-time qRT-PCR

Total RNA was extracted with TRI Reagent® (Sigma-Aldrich) and reverse-transcribed with random primer combined with the ImProm-II™ Reverse Transcription System (Promega). Quantitative

real-time PCR was performed using FastStart Universal SYBR Green Master Mix (Roche) using an Applied StepOnePlus™ Real-Time PCR System (Thermo Fisher Scientific). Gene-specific transcript levels were normalized against human *ACTB* transcript levels. Primer sequences are indicated in Appendix Table S3.

Statistical analysis

Prism 6 (GraphPad) and R (The R foundation) were used for statistical analysis of data. Statistical analysis applied to the results from the CRISPR/Cas9 screen is described above. One-way ANOVA with Dunnett's test for multiple comparison was used to compare the values of WT cells to the values of the various knock-out cells. When comparisons were made with different control groups (e.g. WT untreated or WT treated with IFN-γ), Sidak's correction was applied.

Data availability

The authors declare that the data supporting the findings of this study are available within the paper and its Appendix. The datasets produced in this study are available in the following database (RNA-seq data: Gene Expression Omnibus GSE132178; <https://www.ncbi.nlm.nih.gov/geo/query/acc.cgi?acc=GSE132178>).

Expanded View for this article is available online.

Acknowledgements

We thank B. Fairfax (University of Oxford, U.K.) for providing the IRF2 ChIP-seq data; W. Conlan (NRC, Ottawa, Canada) for *F. novicida* LPS; J. Yuan (Harvard Medical School, USA), B. Py (CIRI, Lyon, France), A. Cimorelli (CIRI, Lyon, France) for providing cDNA and plasmids; and J. Rajwani (University of Calgary) for careful reading of the manuscript. We acknowledge the contribution of SFR Biosciences (UMS3444/CNRS, US8/Inserm, ENS de Lyon, UCBL) cytometry and vectorology facilities. This work was supported by ERC starting grant 311542, an ANR grant (ANR-16-CE15-0011) and an intramural CIRI grant. This work was performed within the framework of the LABEX ECOFACT (ANR-11-LABX-0048) of Université de Lyon, within the program "Investissements d'Avenir" (ANR-11-IDEX-0007) operated by the French National Research Agency (ANR). Experiments done in the laboratory of Dr. Ricci have been supported by the INGESTEM French National infrastructure. GG is supported by a fellowship from the Fondation pour la Recherche Médicale (SPF201809006927).

Author contributions

SB and TH designed the research. SB, GG, MPG, BL, MC, KK, and AM performed the experiments. KK, OA, AC, J-BC, CFB, SH performed the bioinformatics analyses; SH and BG generated the NGS and RNA-seq data. MPG and RR designed and generated the iPSC data. SB and TH wrote the manuscript with input and revisions from all authors.

Conflict of interest

The authors declare that they have no conflict of interest.

References

1. Fleischmann C, Scherag A, Adhikari NKJ, Hartog CS, Tsaganos T, Schlattmann P, Angus DC, Reinhart K (2016) Assessment of global incidence

- and mortality of hospital-treated sepsis. Current estimates and limitations. *Am J Respir Crit Care Med* 193: 259–272
2. Singer M, Deutschman CS, Seymour CW, Shankar-Hari M, Annane D, Bauer M, Bellomo R, Bernard GR, Chiche J-D, Cooper-Smith CM et al (2016) The third international consensus definitions for sepsis and septic shock (Sepsis-3). *JAMA* 315: 801–810
 3. Hotchkiss RS, Monneret G, Payen D (2013) Sepsis-induced immunosuppression: from cellular dysfunctions to immunotherapy. *Nat Rev Immunol* 13: 862–874
 4. Cavaillon J-M (2017) Exotoxins and endotoxins: inducers of inflammatory cytokines. *Toxicol* 149: 45–53
 5. Stinebring WR, Youngner JS (1964) Patterns of interferon appearance in mice injected with bacteria or bacterial endotoxin. *Nature* 204: 712
 6. Sauter C, Wolfensberger C (1980) Interferon in human serum after injection of endotoxin. *Lancet* 2: 852–853
 7. Poltorak A, He X, Smirnova I, Liu MY, Van Huffel C, Du X, Birdwell D, Alejos E, Silva M, Galanos C et al (1998) Defective LPS signaling in C3H/HeJ and C57BL/10ScCr mice: mutations in Tlr4 gene. *Science* 282: 2085–2088
 8. Shi J, Zhao Y, Wang Y, Gao W, Ding J, Li P, Hu L, Shao F (2014) Inflammatory caspases are innate immune receptors for intracellular LPS. *Nature* 514: 187–192
 9. Hagar JA, Powell DA, Aachoui Y, Ernst RK, Miao EA (2013) Cytoplasmic LPS activates caspase-11: implications in TLR4-independent endotoxic shock. *Science* 341: 1250–1253
 10. Kayagaki N, Wong MT, Stowe IB, Ramani SR, Gonzalez LC, Akashi-Takamura S, Miyake K, Zhang J, Lee WP, Muszynski A et al (2013) Noncanonical inflammasome activation by intracellular LPS independent of TLR4. *Science* 341: 1246–1249
 11. Kayagaki N, Warming S, Lamkanfi M, Vande Walle L, Louie S, Dong J, Newton K, Qu Y, Liu J, Heldens S et al (2011) Non-canonical inflammasome activation targets caspase-11. *Nature* 479: 117–121
 12. Shi J, Zhao Y, Wang K, Shi X, Wang Y, Huang H, Zhuang Y, Cai T, Wang F, Shao F (2015) Cleavage of GSDMD by inflammatory caspases determines pyroptotic cell death. *Nature* 526: 660–665
 13. Kayagaki N, Stowe IB, Lee BL, O'Rourke K, Anderson K, Warming S, Cuelar T, Haley B, Roose-Girma M, Phung QT et al (2015) Caspase-11 cleaves gasdermin D for non-canonical inflammasome signalling. *Nature* 526: 666–671
 14. Cookson BT, Brennan MA (2001) Pro-inflammatory programmed cell death. *Trends Microbiol* 9: 113–114
 15. Petrilli V, Papin S, Dostert C, Mayor A, Martinon F, Tschopp J (2007) Activation of the NALP3 inflammasome is triggered by low intracellular potassium concentration. *Cell Death Differ* 14: 1583–1589
 16. Schmid-Burgk JL, Gaidt MM, Schmidt T, Ebert TS, Bartok E, Hornung V (2015) Caspase-4 mediates non-canonical activation of the NLRP3 inflammasome in human myeloid cells. *Eur J Immunol* 45: 2911–2917
 17. Ruhl S, Broz P (2015) Caspase-11 activates a canonical NLRP3 inflammasome by promoting K(+) efflux. *Eur J Immunol* 45: 2927–2936
 18. Fitzgerald KA, Rowe DC, Golenbock DT (2004) Endotoxin recognition and signal transduction by the TLR4/MD2-complex. *Microbes Infect* 6: 1361–1367
 19. Broz P, Dixit VM (2016) Inflammasomes: mechanism of assembly, regulation and signalling. *Nat Rev Immunol* 16: 407–420
 20. Gaidt MM, Ebert TS, Chauhan D, Schmidt T, Schmid-Burgk JL, Rapino F, Robertson AAB, Cooper MA, Graf T, Hornung V (2016) Human monocytes engage an alternative inflammasome pathway. *Immunity* 44: 833–846
 21. Stehlik C, Dorfleutner A (2007) COPs and POPs: modulators of inflammatory activity. *J Immunol* 179: 7993–7998
 22. Khare S, Dorfleutner A, Bryan NB, Yun C, Radian AD, de Almeida L, Rojanasakul Y, Stehlik C (2012) An NLRP7-containing inflammasome mediates recognition of microbial lipopeptides in human macrophages. *Immunity* 36: 464–476
 23. Gavriliu MA, Wewers MD (2011) Francisella Recognition by Inflammasomes: differences between Mice and Men. *Front Microbiol* 2: 11
 24. Chavarria-Smith J, Mitchell PS, Ho AM, Daugherty MD, Vance RE (2016) Functional and evolutionary analyses identify proteolysis as a general mechanism for NLRP1 inflammasome activation. *PLoS Pathog* 12: e1006052
 25. Chae JJ, Centola M, Aksentijevich I, Dutra A, Tran M, Wood G, Nagaraju K, Kingma DW, Liu PP, Kastner DL (2000) Isolation, genomic organization, and expression analysis of the mouse and rat homologs of MEFV, the gene for familial Mediterranean fever. *Mamm Genome* 11: 428–435
 26. Monack DM, Hersh D, Ghori N, Bouley D, Zychlinsky A, Falkow S (2000) Salmonella exploits caspase-1 to colonize Peyer's patches in a murine typhoid model. *J Exp Med* 192: 249–258
 27. Rathinam VAK, Vanaja SK, Waggoner L, Sokolovska A, Becker C, Stuart LM, Leong JM, Fitzgerald KA (2012) TRIF licenses caspase-11-dependent NLRP3 inflammasome activation by gram-negative bacteria. *Cell* 150: 606–619
 28. Vigano E, Diamond CE, Spreafico R, Balachander A, Sobota RM, Mortelaro A (2015) Human caspase-4 and caspase-5 regulate the one-step non-canonical inflammasome activation in monocytes. *Nat Commun* 6: 8761
 29. Yuan J, Najafov A, Py BF (2016) Roles of caspases in necrotic cell death. *Cell* 167: 1693–1704
 30. Lagrange B, Benaoudia S, Wallet P, Magnotti F, Provost A, Michal F, Martin A, Di Lorenzo F, Py BF, Molinaro A et al (2018) Human caspase-4 detects tetra-acylated LPS and cytosolic Francisella and functions differently from murine caspase-11. *Nat Commun* 9: 242
 31. Aachoui Y, Leaf IA, Hagar JA, Fontana MF, Campos CG, Zak DE, Tan MH, Cotter PA, Vance RE, Aderem A et al (2013) Caspase-11 protects against bacteria that escape the vacuole. *Science* 339: 975–978
 32. Napier BA, Brubaker SW, Sweeney TE, Monette P, Rothmeier GH, Gertsch NA, Puschnik A, Carette JE, Khatri P, Monack DM (2016) Complement pathway amplifies caspase-11-dependent cell death and endotoxin-induced sepsis severity. *J Exp Med* 213: 2365–2382
 33. Doench JG, Fusi N, Sullender M, Hegde M, Vaimberg EW, Donovan KF, Smith I, Tothova Z, Wilen C, Orchard R et al (2016) Optimized sgRNA design to maximize activity and minimize off-target effects of CRISPR-Cas9. *Nat Biotechnol* 34: 184–191
 34. Man SM, Karki R, Malireddi RKS, Neale G, Vogel P, Yamamoto M, Lamkanfi M, Kanneganti T-D (2015) The transcription factor IRF1 and guanylate-binding proteins target activation of the AIM2 inflammasome by Francisella infection. *Nat Immunol* 16: 467–475
 35. Karki R, Lee E, Place D, Samir P, Mavuluri J, Sharma BR, Balakrishnan A, Malireddi RKS, Geiger R, Zhu Q et al (2018) IRF8 regulates transcription of naips for NLRC4 inflammasome activation. *Cell* 173: 920–933
 36. Ojcius DM, Zychlinsky A, Zheng LM, Young JD (1991) Ionophore-induced apoptosis: role of DNA fragmentation and calcium fluxes. *Exp Cell Res* 197: 43–49
 37. Hentze H, Lin XY, Choi MSK, Porter AG (2003) Critical role for cathepsin B in mediating caspase-1-dependent interleukin-18 maturation and caspase-1-independent necrosis triggered by the microbial toxin nigericin. *Cell Death Differ* 10: 956–968

38. Stanzani M, Orciuolo E, Lewis R, Kontoyiannis DP, Martins SL, St John LS, Komanduri KV (2005) *Aspergillus fumigatus* suppresses the human cellular immune response via gliotoxin-mediated apoptosis of monocytes. *Blood* 105: 2258–2265
39. Nie C, Luo Y, Zhao X, Luo N, Tong A, Liu X, Yuan Z, Wang C, Wei Y (2014) Caspase-9 mediates Puma activation in UCN-01-induced apoptosis. *Cell Death Dis* 5: e1495
40. Harada H, Fujita T, Miyamoto M, Kimura Y, Maruyama M, Furia A, Miyata T, Taniguchi T (1989) Structurally similar but functionally distinct factors, IRF-1 and IRF-2, bind to the same regulatory elements of IFN and IFN-inducible genes. *Cell* 58: 729–739
41. Ren G, Cui K, Zhang Z, Zhao K (2015) Division of labor between IRF1 and IRF2 in regulating different stages of transcriptional activation in cellular antiviral activities. *Cell Biosci* 5: 17
42. Martinon F, Tschopp J (2007) Inflammatory caspases and inflammasomes: master switches of inflammation. *Cell Death Differ* 14: 10–22
43. Fairfax BP, Humburg P, Makino S, Naranbhai V, Wong D, Lau E, Jostins L, Plant K, Andrews R, McGee C et al (2014) Innate immune activity conditions the effect of regulatory variants upon monocyte gene expression. *Science* 343: 1246949
44. MacMicking JD (2012) Interferon-inducible effector mechanisms in cell-autonomous immunity. *Nat Rev Immunol* 12: 367–382
45. Mancino A, Natoli G (2016) Specificity and function of IRF family transcription factors: insights from genomics. *J Interferon Cytokine Res* 36: 462–469
46. Pilla DM, Hagar JA, Haldar AK, Mason AK, Degrandi D, Pfeffer K, Ernst RK, Yamamoto M, Miao EA, Coers J (2014) Guanylate binding proteins promote caspase-11-dependent pyroptosis in response to cytoplasmic LPS. *Proc Natl Acad Sci USA* 111: 6046–6051
47. Santos JC, Dick MS, Lagrange B, Degrandi D, Pfeffer K, Yamamoto M, Meunier E, Pelczar P, Henry T, Broz P (2018) LPS targets host guanylate-binding proteins to the bacterial outer membrane for non-canonical inflammasome activation. *EMBO J* 37: e98089
48. Rosadini CV, Kagan JC (2017) Early innate immune responses to bacterial LPS. *Curr Opin Immunol* 44: 14–19
49. Finethy R, Luoma S, Orench-Rivera N, Feeley EM, Haldar AK, Yamamoto M, Kanneganti T-D, Kuehn MJ, Coers J (2017) Inflammasome activation by bacterial outer membrane vesicles requires guanylate binding proteins. *mBio* 8: e01188-17
50. Casson CN, Yu J, Reyes VM, Taschuk FO, Yadav A, Copenhaver AM, Nguyen HT, Collman RG, Shin S (2015) Human caspase-4 mediates noncanonical inflammasome activation against gram-negative bacterial pathogens. *Proc Natl Acad Sci USA* 112: 6688–6693
51. Kajiwara Y, Schiff T, Voloudakis G, Gama Sosa MA, Elder G, Bozdagi O, Buxbaum JD (2014) A critical role for human caspase-4 in endotoxin sensitivity. *J Immunol* 193: 335–343
52. Honda K, Taniguchi T (2006) IRFs: master regulators of signalling by Toll-like receptors and cytosolic pattern-recognition receptors. *Nat Rev Immunol* 6: 644–658
53. Tanaka N, Kawakami T, Taniguchi T (1993) Recognition DNA sequences of interferon regulatory factor 1 (IRF-1) and IRF-2, regulators of cell growth and the interferon system. *Mol Cell Biol* 13: 4531–4538
54. Casanova J-L, Abel L (2018) Human genetics of infectious diseases: unique insights into immunological redundancy. *Semin Immunol* 36: 1–12
55. Cuesta N, Salkowski CA, Thomas KE, Vogel SN (2003) Regulation of lipopolysaccharide sensitivity by IFN regulatory factor-2. *J Immunol* 170: 5739–5747
56. Kayagaki N, Lee BL, Stowe IB, Kornfeld OS, O'Rourke K, Mirrashidi KM, Haley B, Watanabe C, Roose-Girma M, Modrusan Z et al (2019) IRF2 transcriptionally induces GSDMD expression for pyroptosis. *Sci Signal* 12: eaax4917
57. van Oost BA, Edgell CJ, Hay CW, MacGillivray RT (1986) Isolation of a human von Willebrand factor cDNA from the hybrid endothelial cell line EA.hy926. *Biochem Cell Biol* 64: 699–705
58. Hedl M, Abraham C (2012) IRF5 risk polymorphisms contribute to interindividual variance in pattern recognition receptor-mediated cytokine secretion in human monocyte-derived cells. *J Immunol* 188: 5348–5356
59. Hedl M, Yan J, Witt H, Abraham C (2019) IRF5 is required for bacterial clearance in human M1-polarized macrophages, and IRF5 immune-mediated disease risk variants modulate this outcome. *J Immunol* 202: 920–930
60. van Wilgenburg B, Browne C, Vowles J, Cowley SA (2013) Efficient, long term production of monocyte-derived macrophages from human pluripotent stem cells under partly-defined and fully-defined conditions. *PLoS ONE* 8: e71098
61. Bolger AM, Lohse M, Usadel B (2014) Trimmomatic: a flexible trimmer for Illumina sequence data. *Bioinformatics* 30: 2114–2120
62. Langmead B, Wilks C, Antonescu V, Charles R (2018) Scaling read aligners to hundreds of threads on general-purpose processors. *Bioinformatics* 35: 421–432
63. Li H, Handsaker B, Wysoker A, Fennell T, Ruan J, Homer N, Marth G, Abecasis G, Durbin R (2009) The Sequence Alignment/Map format and SAMtools. *Bioinformatics* 25: 2078–2079
64. Zhang Y, Liu T, Meyer CA, Eeckhoutte J, Johnson DS, Bernstein BE, Nussbaum C, Myers RM, Brown M, Li W et al (2008) Model-based analysis of ChIP-Seq (MACS). *Genome Biol* 9: R137
65. Quinlan AR, Hall IM (2010) BEDTools: a flexible suite of utilities for comparing genomic features. *Bioinformatics* 26: 841–842
66. Robinson JT, Thorvaldsdottir H, Winckler W, Guttman M, Lander ES, Getz G, Mesirov JP (2011) Integrative genomics viewer. *Nat Biotechnol* 29: 24–26